3

Laser energy absorption in matter

We learned in Chapter 1 that there are two principal ways to add energy to matter to bring the matter up to high temperature and pressure: via absorption of energy from an incident particle or photon beam, or via high-velocity collision with other matter. As for the first mechanism – absorption of energy from an incident particle or photon beam – we also learned in Chapter 1 that it is much easier to focus a photon beam to very high energy density since photons, being electrically neutral, are not subject to the Coulomb forces that act to push apart the charged particles making up an electron or ion beam. Accordingly, lasers are commonly used to create extreme conditions in matter. Indeed, lasers can create a very wide range of extreme conditions. They can also create extreme conditions which cannot be created any other way outside astrophysical objects, except by nuclear detonations.

In this chapter we discuss the physical mechanisms by which the energy in a laser beam is absorbed in matter. The physical mechanisms are different for different laser intensities. We also discuss how the absorbed energy gets converted into material pressure. It is the pressure gradient created in the material by the laser energy absorption that drives the material motions that we discuss in much more detail in the next two chapters.

Before we can understand laser light absorption in matter, though, we need to understand something about the basic nature of electromagnetic radiation and its propagation. This is the topic we address first in the next section.

3.1 Maxwell's equations and electromagnetic wave propagation

The modern era began in the early seventeenth century with the start of the Scientific Revolution. The development of inductive reasoning and the scientific method led directly to the growth of experimental science, starting with the first experiments of Galileo on the mechanics and dynamics of solid bodies. The marriage of experimental science to mathematics after the invention of the calculus by Newton

and Leibnitz in the seventeenth century changed everything. Human understanding of the natural world began to change radically, and the subsequent growth of a technological economy driven by scientific discoveries radically changed the way people lived and worked. If the seventeenth century was the century of great discoveries in the mechanics and dynamics of solid bodies – the century of Galileo and Newton – and the eighteenth century was the century of chemistry and the new understanding of elements and their arrangement into a periodic table, then the nineteenth century was the century of both thermodynamics and electricity and magnetism.

As for thermodynamics, we already met in the previous chapter the great German physicist Ludwig Boltzmann. We learned that his particular insight was to show how the flow of heat in a material could be explained on the basis of a statistical averaging of the random motions of an ensemble of individual atoms in the material.

Here, we meet James Clark Maxwell, an English physicist and contemporary of Boltzmann who was arguably the greatest scientist of the nineteenth century. It was Maxwell's insight that led to the discovery of light as an electromagnetic wave. This discovery opened the path to the early twentieth-century development of quantum theory and relativity theory, developments which provided us with our new understanding of atomic and nuclear structure and the fundamental structure of space and time.

Maxwell's particular insight was how to generalize the individual experimentally determined laws for steady-state electric fields and magnetic fields to account for time-varying fields, and then how to combine these generalized laws mathematically to show that the electric field and the magnetic field can propagate together as a wave at the velocity of light.

To understand what it was that Maxwell did, let us start with the basic laws of electricity and magnetism.

First, Coulomb's law states that the force between any two point electrical charges q_1 and q_2 is proportional to the product of the two charges and inversely proportional to the square of the distance r between them:

$$\mathbf{F}_{12} = \frac{q_1 q_2}{r^2}\hat{\mathbf{r}}, \tag{3.1}$$

where $\hat{\mathbf{r}}$ is a unit vector in the r-direction. We have written equation (3.1) in Gaussian units, where the constant of proportionality is taken to be identically equal to one.

The electric field $\mathbf{E}$ is defined as the force per unit charge. Thus, the electric field of point charge q_1 is

$$\mathbf{E}_1 = \frac{q_1}{r^2}\hat{\mathbf{r}}. \tag{3.2}$$

https://doi.org/10.1017/CBO9781139095150.003 Published online by Cambridge University Press

We can generalize Coulomb's law for a distribution of point electrical charges in three dimensions as

$$\nabla \cdot \mathbf{E} = 4\pi\rho_e, \tag{3.3}$$

where ρ_e is the charge density. Once again, equation (3.3) is written in Gaussian units. An excellent discussion of the various systems of units for electromagnetism, and how to convert from one system of units to another, is given in an appendix to Jackson's 1962 text *Classical Electrodynamics* listed in the Further Reading.

Electric current is defined as the time rate of change of electric charge, that is, $I = dq/dt$. Thus, the ratio of the charge to the current has dimensions of time. With these definitions, we can now write a continuity equation for the charge density ρ_e and current density $\mathbf{J}$:

$$\nabla \cdot \mathbf{J} + \frac{\partial \rho_e}{\partial t} = 0. \tag{3.4}$$

Next, let us consider Ampere's law. This law states that the force per unit length between two infinitely long parallel conductors separated by a distance R is proportional to the product of the currents in the two wires and inversely proportional to R. See equation (1.6), which is a mathematical expression of Ampere's law. We first introduced this law in discussing how a Z-pinch device works.

The magnetic field $\mathbf{B}$ is defined as the force per unit current. Thus, writing equation (1.6) in three dimensions, and again using Gaussian units, in which the magnetic permeability of free space is $\mu_0 = 1$, we can rewrite Ampere's law as

$$\nabla \times \mathbf{B} = \frac{4\pi}{c}\mathbf{J}. \tag{3.5}$$

Maxwell was the first to recognize that Ampere's law as written in equation (3.5) applies only to a steady-state current flow, and thus implies that the divergence of the current density vanishes, that is, $\nabla \cdot \mathbf{J} = 0$. This is easy to see from equation (3.5), since the divergence of the curl of any vector quantity is identically zero. From the charge conservation equation, equation (3.4), we see that the divergence of the current density is zero only for steady-state flow, that is, flow for which $\partial\rho_e/\partial t = 0$. Maxwell realized that he could generalize Ampere's law for time-varying electric and magnetic fields, and still be consistent with the conservation relation, if he simply substituted Coulomb's law into the conservation equation. Thus,

$$\nabla \cdot \mathbf{J} + \frac{\partial \rho_e}{\partial t} = \nabla \cdot \left(\mathbf{J} + \frac{1}{4\pi}\frac{\partial \mathbf{E}}{\partial t} \right). \tag{3.6}$$

Substituting the expression in parentheses in equation (3.6) for the current density in equation (3.5) then yields Maxwell's generalization of Ampere's law for

time-varying fields:

$$\nabla \times \mathbf{B} = \frac{4\pi}{c}\mathbf{J} + \frac{1}{c}\frac{\partial \mathbf{E}}{\partial t}. \tag{3.7}$$

Maxwell called the second term in parentheses in equation (3.6) the displacement current density. The first term, **J**, is the conduction current density.

The third and final experimental relation that Maxwell considered is Faraday's law of induction, which connects the electric field to a time-varying magnetic field. Faraday's observation was that the electric force induced around a closed electric current path is proportional to the time rate of change of magnetic flux through the area contained within the closed current path. Faraday's law is expressed mathematically as

$$\nabla \times \mathbf{E} + \frac{1}{c}\frac{\partial \mathbf{B}}{\partial t} = 0. \tag{3.8}$$

Up to now we have considered only electric and magnetic fields in free space. Electric and magnetic fields in a material medium are modified by the electric and magnetic properties of the individual atoms in the particular material. These properties are characterized by two constants. The dielectric permittivity ϵ is the proportionality constant between the electric field in the material and the external (free-space) electric field:

$$\mathbf{D} = \epsilon \mathbf{E}. \tag{3.9}$$

Likewise, the magnetic permeability μ is the proportionality constant between the magnetic field in the material and the external (free-space) magnetic field:

$$\mathbf{B} = \mu \mathbf{H}. \tag{3.10}$$

Equations (3.9) and (3.10) are valid only in a linear and isotropic material. In the more general case of a material in which the electric field induces a polarization of the atoms – that is, the center of mass of the atomic nucleus becomes offset from the center of mass of the atom's electron cloud in the direction of the electric field – an additional term gets added to equation (3.9) to account for the polarization **P**:

$$\mathbf{D} = \epsilon \mathbf{E} + 4\pi \mathbf{P}. \tag{3.11}$$

Likewise, in the case where the electric field causes all the electron orbital rotation vectors to align, an additional term gets added to equation (3.10) to account for the magnetization **M**:

$$\mathbf{H} = \frac{1}{\mu}\mathbf{B} - 4\pi \mathbf{M}. \tag{3.12}$$

We will not further consider polarization or magnetization. The interested student can learn more about these material properties in most texts on electromagnetism, such as *Classical Electrodynamics* by Jackson already mentioned.

Finally, using equations (3.9) and (3.10), we can now write the four Maxwell equations in Gaussian units in the following way:

$$\nabla \cdot \mathbf{D} = 4\pi\rho_e. \tag{3.13}$$

$$\nabla \times \mathbf{H} = \frac{4\pi}{c}\mathbf{J} + \frac{1}{c}\frac{\partial \mathbf{D}}{\partial t}, \tag{3.14}$$

$$\nabla \cdot \mathbf{B} = 0, \tag{3.15}$$

$$\nabla \times \mathbf{E} + \frac{1}{c}\frac{\partial \mathbf{B}}{\partial t} = 0. \tag{3.16}$$

Equation (3.15) is simply a mathematical expression of the non-existence of magnetic monopoles. That expression, along with Maxwell's generalization of Coulomb's law [equation (3.13)], Ampere's law [equation (3.14)], and Faraday's law [equation (3.16)], constitutes the four Maxwell equations.

Maxwell's next brilliant insight was to see that in the vacuum – that is, in regions where there are no charges and currents – if we take the curl of equation (3.14) and then substitute equation (3.16) for the last term we get a wave equation:

$$\nabla^2\mathbf{B} - \frac{1}{c^2}\frac{\partial^2 \mathbf{B}}{\partial t^2} = 0. \tag{3.17}$$

An identical wave equation can be written for the electric field. Thus, the electric and magnetic fields propagate together as a wave in vacuum at the velocity c, the velocity of light (equal to 2.998×10^{10} cm s^{-1}). In a material medium one can easily show that the electromagnetic wave propagates with velocity

$$c' = \frac{1}{\sqrt{\epsilon\mu}} < c. \tag{3.18}$$

The plane-wave solution of equation (3.17) is

$$\mathbf{B} = \mathbf{B}_0 e^{i\mathbf{k}\cdot\mathbf{r} - i\omega t}, \tag{3.19}$$

with a similar expression for the electric field. The wave of angular frequency ω propagates in the r-direction, with the magnitude of the wave vector given by

$$k = \sqrt{\epsilon\mu}\frac{\omega}{c}. \tag{3.20}$$

In a dispersive medium, ϵ and μ are complex numbers and functions of wavenumber k.

A laser beam can be considered as a propagating planar electromagnetic wave of a particular angular frequency ω. The energy contained in the propagating wave

is proportional to the square of the electric field. The intensity of the laser beam incident on the target material, I_L, is defined as the beam power (energy per unit time) divided by the cross-sectional area of the propagating beam; it has become customary to express laser beam intensity in units of watts per square centimeter (W cm^{-2}). As we first pointed out in Chapter 1, laser beam intensity has different units from what is normally meant by intensity of electromagnetic radiation. In order not to confuse the two different definitions of intensity with one another, we use the subscript L whenever we are referring to the laser beam intensity.

Propagation of the electromagnetic wave in the matter on which it is incident depends on the material constants ϵ and μ. Some of the energy in the electromagnetic wave is transferred to free and bound electrons in the material through which it is propagating. The absorption of the energy of the propagating – and perhaps dispersing – wave depends on the material's temperature and density, and is described by an absorption coefficient κ. The attenuation of the beam intensity along the beam path s in the material is

$$\frac{dI_L}{ds} = -\kappa I_L. \tag{3.21}$$

The fraction of the beam intensity that is absorbed is thus

$$f_a = 1 - \exp\left(-\int \kappa ds\right). \tag{3.22}$$

Since the laser beam is a plane electromagnetic wave in which the electric and magnetic fields oscillate back and forth at the laser light frequency as the wave propagates, the beam energy is absorbed by transferring energy to free and/or bound electrons in the material. Some of the electron energy is then transferred to the ions via electron–ion collisions, as discussed in the previous chapter, or electron–neutral collisions. The consequent heating of the electrons and ions (or neutral atoms) then implies an increase in the material pressure. The increased pressure in the laser beam deposition region then drives material motion, both inward and outward.

The dependence of pressure on beam intensity is different in different beam intensity ranges, because the mechanisms by which the beam energy is absorbed – and hence the absorption coefficients – are different in the different beam intensity regimes. For the purposes of the following discussion, we consider three ranges of beam intensity – high intensity, low intensity, and very low intensity. We show in this chapter that the relationship between pressure and beam intensity is approximately as shown in Figure 3.1, with the understanding that the boundaries between these regimes are not as sharp and well-defined as portrayed in the figure.

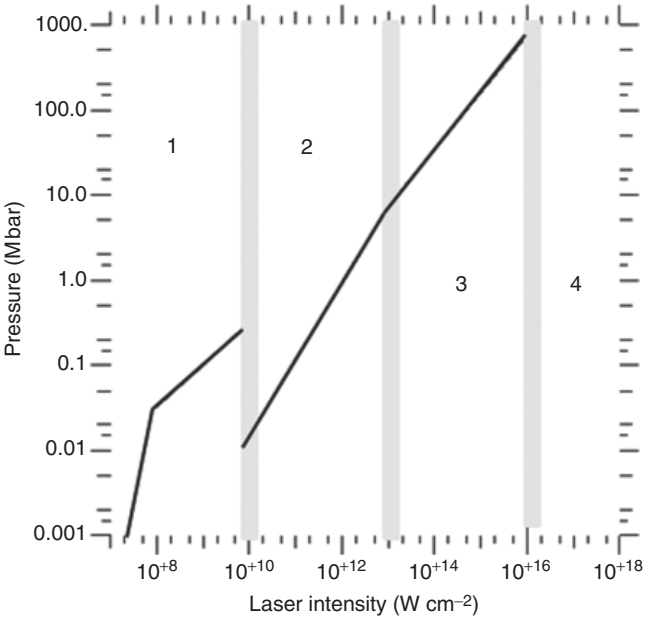

Figure 3.1 Approximate relation between material pressure and incident laser beam intensity: 1, regime of tamped ablation; 2, collisional absorption regime; 3, collisionless absorption regime; 4, relativistic regime.

3.2 Laser energy deposition at high laser intensities

For laser beam intensities above about 10^{13} W cm^{-2}, the high-intensity regime, the laser beam deposits its energy into the material and creates matter that has a wide range of extreme conditions, as illustrated in Figure 1.1. The three regions illustrated in Figure 1.1 – the region of classical or collisionless plasma, the region of collisional plasma, and the region of dense or degenerate plasma – are created very rapidly (i.e., in a time that is short compared to the pulse duration), and the laser beam then interacts with the collisionless coronal plasma, Region 1 in Figure 1.1. In this section we discuss the physical mechanisms by which the laser beam energy is deposited in this coronal plasma.

3.2.1 Inverse bremsstrahlung absorption

The main characteristic of the coronal plasma is that it consists of material that is partially or fully ionized. That is, some or all of the atom's electrons have been liberated from their orbits and are now free. We discuss the ionization physics in more detail in Chapter 7. There we will learn how to calculate the average degree of ionization, Z^*, as a function of electron temperature T_e, electron density n_e, and

https://doi.org/10.1017/CBO9781139095150.003 Published online by Cambridge University Press

the ionization potentials of the various quantum electron energy levels in the atom. For the purposes of our discussion here, let us assume we already know Z^*.

The key point here is that, since the photon energy is generally small compared to the ionization potentials, the interaction of the laser light with the plasma is dominated by interactions of the photons with free electrons. This interaction is the inverse of the bremsstrahlung process.

In the bremsstrahlung process, electromagnetic radiation is emitted whenever a free electron is decelerated as it is passing by – and influenced by the electric field of – a nearby ion. The energy of the emitted photon is equal to the energy the electron loses in its deceleration. Averaging over the Maxwell–Boltzmann distribution of electron energies in plasma with electron temperature T_e, we find that hot plasma emits a spectrum of radiation as a result of these free–free transitions. This emitted radiation is called bremsstrahlung, the German word for braking radiation. The bremsstrahlung spectrum is a function of T_e, the electron density n_e, and the ion density $n_i = n_e/Z^*$.

The absorption of high-intensity laser light in coronal plasma is the inverse of this process. The photons accelerate the electrons in the vicinity of the ions. Thus, the energy of the laser beam is given to the free electrons in free–free inverse bremsstrahlung transitions.

Once again, averaging over a Maxwell–Boltzmann thermal distribution of free electron energies, we find that we can write the inverse bremsstrahlung absorption coefficient, in units of cm^{-1}, as

$$\kappa_{IB} = \sqrt{2\pi}\frac{16\pi}{3}\frac{(Z^*)^2 n_e n_i e^6 \ln(\Lambda_{ei})}{c\,(m_e k T_e)^{3/2}\,\omega_0^2\sqrt{\epsilon}}, \tag{3.23}$$

where e is the electron charge, m_e the electron mass, ω_0 the laser angular frequency, $\ln(\Lambda_{ei})$ the Coulomb logarithm (a function of the collision impact parameter introduced in Chapter 2 and discussed in more detail in Chapter 8), and where the dielectric permittivity is given by

$$\epsilon = 1 - \frac{\omega_{pe}^2}{\omega_0^2}, \tag{3.24}$$

with ω_{pe} the electron plasma frequency, defined just after equation (2.97).

Note from equations (3.23) and (3.24) that the inverse bremsstrahlung absorption coefficient is a real number only for laser light frequencies greater than the electron plasma frequency. Another way of saying this is that the laser light can propagate and absorb only in plasma less dense than the critical density, that is, in classical or collisionless plasma.

The rate at which the laser beam deposits its energy via inverse bremsstrahlung is approximately equal to the rate the electron plasma is heated, which, in turn,

is proportional to the electron–ion collision frequency. This collision frequency, according to equation (2.80) derived in the previous chapter, is proportional to $T_e^{-3/2}$. Thus, this same dependence on electron temperature is reflected in the expression for inverse bremsstrahlung absorption, equation (3.23). This dependence implies that the absorption by inverse bremsstrahlung increases as electron temperature decreases. The inverse bremsstrahlung absorption preferentially heats the lower-energy electrons, keeping the plasma close to thermodynamic equilibrium.

Further, we can see from equations (3.23) and (3.24) that the absorption increases the closer the electromagnetic wave penetrates to the critical density. The critical density is inversely proportional to the square of the laser wavelength,

$$n_c \left(\mathrm{cm}^{-3}\right) = 8.8 \times 10^{20} / \left[\lambda\,(\mu\mathrm{m})\right]^2 . \tag{3.25}$$

Thus, the position of the critical density in the coronal plasma is different for different wavelengths of laser light. In particular, the critical density for the 1.06-μm laser light produced by a Nd-doped glass laser is 100 times greater than for the 10.6-μm laser light produced by a CO_2 gas laser. This means that the 1-μm light penetrates deeper into the coronal plasma, closer to the original target surface, at which there is much more absorption of the laser beam energy.

If the laser beam intensity is sufficiently high, the strong electric field of the electromagnetic wave distorts the electron distribution, which modifies the collision frequency. Thus, the inverse bremsstrahlung absorption coefficient becomes dependent on intensity. The beam intensity at which absorption becomes non-linear is the intensity at which the electron quiver velocity v_0 becomes comparable to the electron thermal velocity v_{th}^e.

Let us define a non-dimensional parameter

$$\alpha = \frac{Z^* v_0^2}{\left(v_{th}^e\right)^2}. \tag{3.26}$$

B. Langdon showed in 1980 that, at very high laser intensities, the inverse bremsstrahlung absorption coefficient given by equation (3.23) is modified (reduced) by a multiplicative factor

$$f = 1 - \frac{0.533}{1 + \left(\frac{0.27}{\alpha}\right)^{3/4}}, \tag{3.27}$$

with the electron quiver velocity given by

$$v_0 = \frac{e}{m_e \omega_0}\sqrt{\frac{8\pi}{c} I_L}, \tag{3.28}$$

https://doi.org/10.1017/CBO9781139095150.003 Published online by Cambridge University Press

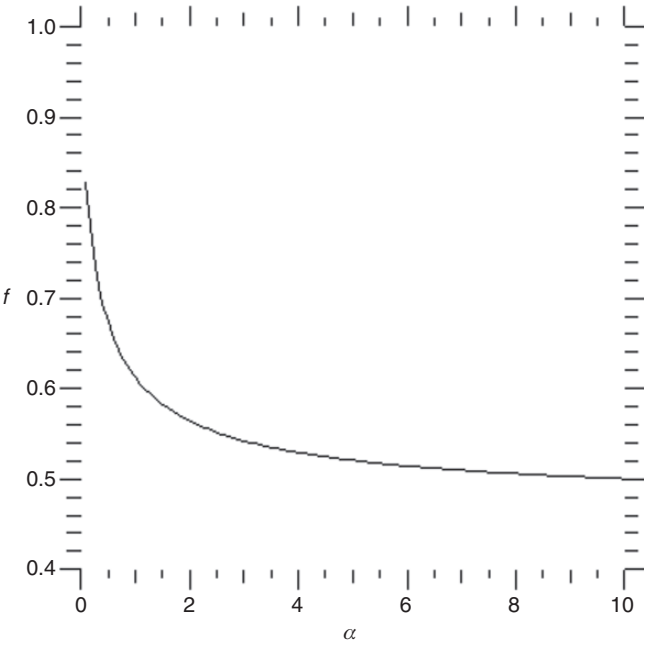

Figure 3.2 The inverse bremsstrahlung absorption reduction factor as a function of the parameter α, which is approximately the ratio of the electron quiver energy to its thermal energy.

and the laser beam intensity I_L in units of W cm^{-2}. The inverse bremsstrahlung absorption reduction factor is plotted as a function of the parameter α in Figure 3.2.

3.2.2 Resonance absorption

As we saw in the previous subsection, an electromagnetic wave propagating through under-dense plasma – that is, plasma with a density less than the critical density – deposits its energy along the beam path via inverse bremsstrahlung absorption. Beam energy that is left at the time the beam arrives at the critical-density surface, with the critical density given by equation (3.25), may be absorbed via resonance absorption. In this process, the electromagnetic wave couples with a longitudinal electron plasma wave. We discussed electron plasma waves in Chapter 2; there, we learned that the electron plasma wave has a frequency equal to the electron plasma frequency. The process is called resonance absorption because the oscillation of the electric field of the electromagnetic wave is in resonance with the oscillation of the electrons in the electron plasma wave. The resonant coupling cannot occur, however, unless the electric field vector has a component in the direction of the

density gradient. Thus, the light beam must be oblique to the surface of the plasma. Even then, it cannot have a linear polarization parallel to the plasma surface, for in that case coupling will not take place, and the wave will be specularly reflected.

An electromagnetic wave incident at an angle θ to the surface does not reflect right at the critical-density surface, but at the lower density $n_c \cos^2 \theta$. Some of the beam energy quantum-mechanically tunnels its way to the critical-density surface, and the remainder is specularly reflected. The reflection point is called the turning point. For plasma with a steep density gradient, the turning point and the critical-density point are close together, and the resonance absorption is very efficient.

The resonance absorption efficiency is a function of the angle of incidence and the density-gradient scale length. If the angle of incidence is too large, the beam will be reflected too far away from the critical-density surface. If the incidence angle is too small, the component of the electric field vector parallel to the density gradient is too small at the turning point.

Vitaly Ginsburg showed in 1970 that the resonance absorption fraction is

$$f_{ra} = \frac{1}{2}\phi^2(\tau), \tag{3.29}$$

with

$$\phi(\tau) = 2.10\tau e^{-\frac{2}{3}\tau^3} \tag{3.30}$$

and

$$\tau = (k_0 L)^{1/3} \sin\theta. \tag{3.31}$$

In equation (3.31), k_0 is the wavenumber of the incident electromagnetic wave and $L = n_e/\nabla n_e$ is the electron density-gradient scale length. In Figure 3.3 we show a plot of the resonance absorption fraction as a function of the dimensionless electron density-gradient scale length for a beam incidence angle of 20°.

The electron density scale length can be expressed as some multiple of the electron Debye length, which is given by the second term in equation (2.86). Thus, L is proportional to $\sqrt{T_e/n_e}$.

As for inverse bremsstrahlung absorption considered in the previous subsection, if the laser beam intensity is sufficiently high, the strong electric field of the electromagnetic wave distorts the electron distribution, so the resonance absorption process is modified. At beam intensities above about 10^{18}–10^{19} W cm^{-2} the quiver velocity of the electrons in the electromagnetic field of the laser beam becomes relativistic, so the electron mass distribution oscillates in a non-linear way. Hence, the critical density is modified. It is beyond the scope of the current text to discuss in detail relativistic effects in plasma; this topic alone would require a whole additional

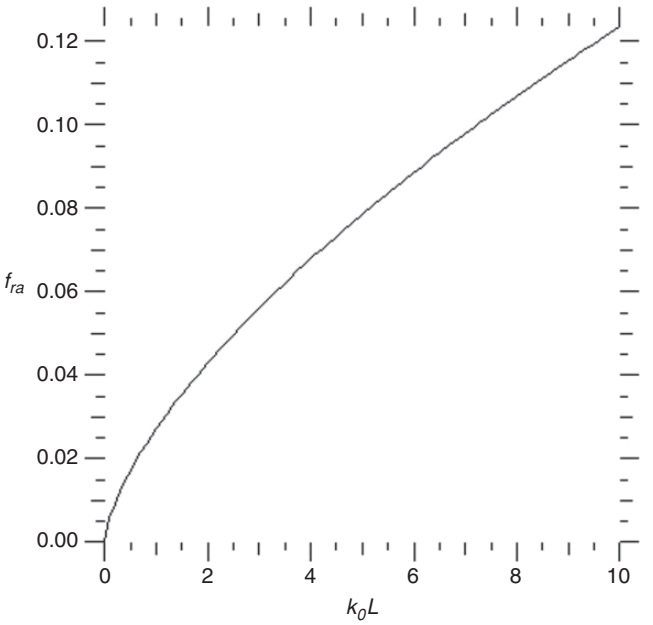

Figure 3.3 The resonance absorption fraction as a function of the dimensionless electron density scale length for a beam incidence angle of 20°.

book. We simply point out here that in relativistic plasma we can estimate the critical electron density for resonance absorption as

$$n_c \cong n_{c0}\left(1 + \frac{I_L\lambda^2\left(\mathrm{W\,cm^{-2}\,\mu m^2}\right)}{f_c \times 10^{18}}\right)^{1/2}, \tag{3.32}$$

a formulation first introduced by J.R. Davies in 2008. In equation (3.32) n_{c0} is the non-relativistic critical density given by equation (3.25), and the factor f_c can be obtained from fits to measurements and typically has a value between 1 and 3. We see from equation (3.32) that at the ultra-high laser beam intensities produced by short-pulse lasers, the critical density at which resonance absorption takes place can be a factor of several tens greater than the non-relativistic critical density.

In summary, high-intensity laser light propagates through classical plasma, depositing its energy via inverse bremsstrahlung along the beam path. When whatever is left of the beam energy arrives at the turning point, some of the remaining beam energy is absorbed via the resonance absorption process, and the remainder is reflected. The reflected energy, in its travel back out through the coronal plasma, is then subject to more inverse bremsstrahlung absorption. Some fraction of the incident energy may be reflected back out, escaping absorption entirely.

3.2.3 Ponderomotive force and ablation pressure

Photons are massless, but nonetheless laser light does exert a radiation pressure; the free-space radiation pressure is equal to one-third the free-space radiation energy density. Normally, radiation energy density is small compared to the energy density in the plasma particles. At high intensity, however, the laser light can have a radiation pressure comparable to the plasma pressure, particularly in those regions near the critical density where the velocity of the electromagnetic wave is less than c and resonance absorption causes the plasma to expand.

These regions are also characterized by an electron density gradient. When the electron density gradient is steep – that is, the electron density-gradient scale length is short and the resonance absorption is high – there exists a steep gradient in the radiation pressure. This is particularly true when the density-gradient scale length is comparable to the wavelength of the laser light. This pressure gradient produces a ponderomotive force which can result in motion of the plasma particles.

The resulting motion can alter the plasma density profile, which in turn can modify the absorption characteristics of the plasma. Thus, in order to calculate accurately the absorption of high-intensity laser light in classical plasma, we must account for the effects of the ponderomotive force in altering the electron and ion densities in the laser energy deposition region close to the critical density.

The radiation pressure in the plasma is

$$P_R = \frac{1}{2c}\left[\frac{1}{\sqrt{\epsilon}} - \sqrt{\epsilon}\right] I_L. \tag{3.33}$$

The ponderomotive force is the negative of the pressure gradient. Note that in free space $\epsilon = 1$ and the radiation pressure given by equation (3.33) vanishes.

Finally, let us consider the scaling of the pressure with the incident laser intensity in the under-dense coronal plasma. The laser beam, as discussed above, preferentially heats the lower-energy electrons, keeping the coronal plasma close to thermodynamic equilibrium and isothermal. Since most of the beam energy is absorbed at or near the critical density, we can write

$$I_L \propto n_c T_e v_{th}^e, \tag{3.34}$$

where v_{th}^e is the electron thermal velocity. Noting that $v_{th}^e \propto \sqrt{T_e}$, and using equation (3.25), we find that

$$P \propto T_e \propto \left(I_L \lambda^2\right)^{2/3}. \tag{3.35}$$

Thus, for a given laser wavelength λ, the pressure driving the blow-off, or ablation, of the coronal plasma – the ablation pressure – scales as the two-thirds power of the laser intensity. This scaling has been confirmed with detailed numerical

https://doi.org/10.1017/CBO9781139095150.003 Published online by Cambridge University Press

simulations, which also show that this scaling holds for laser intensities above about 10^{13} W cm^{-2}, as shown in Figure 3.1. This scaling has also been confirmed by experiment.

High laser intensity can produce pressures high enough to drive implosion of a thin spherical shell of material to high enough implosion velocity to create the temperature and density conditions necessary for inertial confinement fusion (ICF). Most high-power lasers devoted to this purpose focus the laser light to intensities of a few times 10^{14} to a few times 10^{15} W cm^{-2}, achieving a few hundred Mbar ablation pressures in low-Z ablator shells, like polystyrene or beryllium. The interested student can learn much more about the physics of ICF in John Lindl's monograph *Inertial Confinement Fusion*, listed in the Further Reading.

Let us look back at Figure 1.3 in Chapter 1, which shows the position in temperature–density space of many natural and man-made classical and dense plasmas. There we see that stellar cores and the interior of white dwarf stars are at temperature and density conditions similar to those in an ICF capsule. Thus, high laser intensity can also be used to create plasmas that are scaled versions of such astrophysical plasmas. High laser intensities can also create scaled dynamical astrophysical plasmas, like the ejecta of nova and supernova explosions, bi-polar jets created in the disc accretion process, and stellar wind outflows. Indeed, the development of high-power lasers, as discussed in Chapter 1, has led to the blossoming in the last decade or two of the new subfield of experimental astrophysics. There is a great deal yet to be learned about the physical workings of the universe that can be learned by thoughtful application of laser experiments designed using the computational techniques discussed in this book.

3.3 Laser energy deposition at low laser intensities

For laser intensities above about 10^{13} W cm^{-2}, the high-intensity regime, we saw in the previous section that the laser beam creates and interacts with collisionless coronal plasma. In this regime the ablation pressure scales as the two-thirds power of the laser intensity. Since this is the regime of ICF – as well as experimental astrophysics – it has been well studied, both computationally and experimentally.

Likewise, the regime of very low laser intensity, below about 10^{10} W cm^{-2}, has been well studied. As we will see in the next section, in this regime of intensity, the laser beam interacts largely with a solid, a liquid, a vapor, or very cool plasma.

It is the intermediate-intensity regime, with intensities between about 10^{10} W cm^{-2} and 10^{13} W cm^{-2}, that has not been well studied. In this intensity regime the laser interacts largely with collisional plasma. This is because, at these much lower laser intensities, the ablation pressure and mass ablation rate are much less. Thus, there is much less mass forming the blow-off coronal plasma, and

the laser beam largely deposits its energy in collisional plasma very close to the original solid or liquid surface of the material on which it is incident.

The laser beam heats collisional plasma differently from collisionless plasma. We saw in the previous section that collisionless plasma, in which the electron–ion collision rate is less than the electron plasma frequency, is, to a very good approximation, isothermal. The electron temperature in this isothermal plasma can be approximated by using an electron flux limit in solving the electron thermal transport equation, which is discussed in more detail in Chapter 8.

This approximation is not valid in collisional plasma, so scaling of ablation pressure with laser intensity is different in this low-laser-intensity regime from that in the high-laser-intensity regime. Deriving a scaling relation for the low-intensity regime is non-trivial, and we will not attempt it here. Instead, we will refer to the results of simulations and experiments.

Simulations and experiments published by Colvin and Kalantar in 2006 for a wide range of lasers of different wavelengths and targets made from different materials have shown that the pressure is approximately linear with the laser intensity in the collisional regime. In particular, a power-law fit to simulation results gives

$$P = 41.5 \left[\frac{I_L \left(\mathrm{W\ cm^{-2}} \right)}{3.16 \times 10^{10}} \right]^{0.9} \left(\frac{\lambda_0}{\lambda} \right)^{\alpha(\lambda)} \mathrm{kbar}, \tag{3.36}$$

where λ is the laser wavelength and $\lambda_0 = 1/3$ μm. Note that the scaling exponent for wavelength is itself wavelength-dependent.

Note also that typical pressures generated in the material by these low laser intensities are on the order of a few hundred kbar rather than the few hundred Mbar generated at high laser intensities. Accordingly, these laser intensities are suitable for driving shock waves into solids and liquids to determine the equation of state at conditions relevant to planetary interiors, for example. These laser intensities are also used to study the constitutive properties and response of solid materials at high pressure. We discuss in detail the physics of shock waves and shocks in solids in Chapter 5.

3.4 Laser energy deposition at very low laser intensities

At very low laser intensities – intensities less than about 10^{10} W cm^{-2} – there is generally no ionization and hence no (or very little) coronal plasma. The electromagnetic wave then interacts with the bound electrons in the solid or liquid. The interaction is different for conducting materials, like metals, that have electrons in the conduction band of the atoms, from that for dielectric materials, which have

only bound electrons at energies below the band-gap energy. We consider these two cases in turn.

3.4.1 Conductivity and skin depth

A conducting material is characterized by a conductivity σ in addition to its dielectric permittivity ϵ and magnetic permeability μ. According to Ohm's law, the conductivity is the ratio of the current density to the electric field, that is,

$$\mathbf{J} = \sigma \mathbf{E}. \tag{3.37}$$

Let us now substitute equations (3.9), (3.10), and (3.37) into Maxwell's equations, equations (3.13) through (3.16). We can then write Maxwell's equations for the electromagnetic wave in the conducting material as

$$\nabla \cdot \epsilon \mathbf{E} = 0, \tag{3.38}$$

$$\nabla \times \mathbf{H} - \frac{\epsilon}{c}\frac{\partial \mathbf{E}}{\partial t} - \frac{4\pi\sigma}{c}\mathbf{E} = 0, \tag{3.39}$$

$$\nabla \cdot \mu \mathbf{H} = 0, \tag{3.40}$$

$$\nabla \times \mathbf{E} + \frac{\mu}{c}\frac{\partial \mathbf{H}}{\partial t} = 0. \tag{3.41}$$

Then, for a planar electromagnetic wave, for which the electric and magnetic fields oscillate in space and time as given in equation (3.19), equation (3.39) becomes

$$i\,(\mathbf{k} \times \mathbf{H}) + i\frac{\epsilon\omega}{c}\mathbf{E} - \frac{4\pi\sigma}{c}\mathbf{E} = 0, \tag{3.42}$$

and equation (3.41) becomes

$$\mathbf{k} \times \mathbf{E} + \frac{\mu\omega}{c}\mathbf{H} = 0. \tag{3.43}$$

Once again, $\mathbf{k}$ is the wavenumber of the electromagnetic wave. Now, solving equation (3.43) for $\mathbf{H}$ and substituting the resulting equation for $\mathbf{H}$ into equation (3.42), we find that

$$\left[k^2 - \left(\mu\epsilon\frac{\omega^2}{c^2} + 4\pi i\frac{\mu\omega\sigma}{c^2}\right)\right]\mathbf{E} = 0. \tag{3.44}$$

Equation (3.44) says that the wavenumber of the electromagnetic wave propagating in a conducting material, such as a metal, is a complex number:

$$k = \sqrt{\mu\epsilon}\frac{\omega}{c}\left[\frac{\sqrt{1+\left(\frac{4\pi\sigma}{\omega\epsilon}\right)^2}+1}{2}\right]^{1/2} + i\sqrt{\mu\epsilon}\frac{\omega}{c}\left[\frac{\sqrt{1+\left(\frac{4\pi\sigma}{\omega\epsilon}\right)^2}-1}{2}\right]^{1/2}. \tag{3.45}$$

https://doi.org/10.1017/CBO9781139095150.003 Published online by Cambridge University Press

Substituting equation (3.45) into equation (3.19) we see that the electromagnetic wave propagating in a conducting material is damped. The distance over which the electric and magnetic fields of the electromagnetic wave are attenuated by $1/e$ is equal to the reciprocal of the imaginary part of k, the second term in equation (3.45).

For a good conductor – that is, a conductor for which $4\pi\sigma/\omega\epsilon \gg 1$ – we find that the e-folding attenuation depth δ for the electromagnetic wave is

$$\delta \approx \frac{c}{\sqrt{2\pi\omega\mu\sigma}}. \tag{3.46}$$

This attenuation distance is called the material's skin depth. Very little electromagnetic wave energy penetrates into the conductor to any depth much greater than the skin depth. For a wide range of conducting metals, the skin depth for 1/3-μm laser light is quite small, on the order of a few to a few tens of nanometers. In simulations, it is reasonable to assume that all the absorption of the laser light takes place in the first computational zone right at the surface of the material. This assumption is not reasonable, of course, for materials that have a thickness comparable to the skin depth.

3.4.2 Electromagnetic wave absorption in metals

The fraction of the laser beam energy that is absorbed by the metal is given by

$$f_m = 1 - \left|\frac{n-1}{n+1}\right|^2, \tag{3.47}$$

where n is the index of refraction

$$n = \frac{c}{\omega}k. \tag{3.48}$$

Since k is a complex number – see equation (3.43) – the index of refraction is also a complex number. We leave it as an exercise for the student to show that, if we substitute equation (3.43) for k into equation (3.48), we find that we can write

$$n^2(\omega, T) = \mu\epsilon\left[1 + i\frac{4\pi}{\omega\epsilon}\sigma(\omega, T)\right]. \tag{3.49}$$

In general, as we will see below, the conductivity depends on the angular frequency of the incident wave and on the material temperature. Now it is left for us to derive an expression for the metallic conductivity.

A simple model for metallic conductivity was developed by Drude in 1900. In the Drude model, the conduction electrons in the metal are freely accelerated by the electric field of the incident electromagnetic wave, and decelerated by collisions

with the neutral atoms as well as with lattice vibrations. An equation of motion can therefore be written for the motion of the conduction electrons from Newton's second law of motion:

$$m_e \frac{dv_e}{dt} + m_e \nu_0 v_e = e\mathbf{E}(\mathbf{r}, t), \tag{3.50}$$

where m_e is the electron mass, v_e the electron velocity, e the electron charge, and ν_0 an average electron–neutral collision rate, which we take to be

$$\nu_0 = n_0 \left(\frac{kT}{m_e}\right)^{1/2} \Sigma_0, \tag{3.51}$$

with n_0 the atom number density and Σ_0 the electron–neutral collision cross-section, which is of order 10^{-16} cm^{-2}. The first term on the left-hand side of equation (3.50) is the acceleration term, and the second is the deceleration term, with the applied force being given by the term on the right-hand side.

Substituting the analog of equation (3.19) for the planar electric field into equation (3.50), and assuming that the displacement of the electron from its equilibrium position is small compared to the wavelength of the light in the rapidly oscillating electric field, we can rewrite equation (3.50) as

$$m_e \frac{dv_e}{dt} + m_e \nu_0 v_e = e\mathbf{E}_0 e^{-i\omega t}, \tag{3.52}$$

with $\mathbf{E}_0$ the electric field at the equilibrium position of the electron. The steady-state solution of this ordinary differential equation, equation (3.52), is

$$v_e = \frac{e}{m_e(\nu_0 - i\omega)} \mathbf{E}_0 e^{-i\omega t}. \tag{3.53}$$

Now, we can write Ohm's law, equation (3.37), as

$$e n_e v_e = \sigma E, \tag{3.54}$$

where n_e is the electron density. Solving equation (3.54) for σ and substituting equation (3.53) into the resulting equation, we find that we can write the conductivity as

$$\sigma = n_e \frac{e^2}{m_e \omega \left(\frac{\nu_0}{\omega} - i\right)} = \frac{\omega_{pe}^2}{4\pi\omega \left(\frac{\nu_0}{\omega} - i\right)}, \tag{3.55}$$

where in the last step we used the definition of the electron plasma frequency ω_{pe} given in equation (2.97).

https://doi.org/10.1017/CBO9781139095150.003 Published online by Cambridge University Press

Finally, let us multiply the numerator and denominator of equation (3.55) by $(\nu_0/\omega + i)$. This operation allows us to rewrite equation (3.55) in the form of a complex number as

$$\sigma = \frac{\omega_{pe}^2}{4\pi\omega\left(\frac{\nu_0^2}{\omega^2}+1\right)}\left(\frac{\nu_0}{\omega}+i\right). \tag{3.56}$$

Equation (3.56) is the conductivity of metals given by the Drude model, and provides a reasonably good approximation for metallic conductivity for a wide variety of metals over a wide range of temperatures. Note that metallic conductivity is, in general, a complex number.

For electromagnetic wave angular frequencies small compared to the electron–neutral collision frequency – that is, $\omega \ll \nu_0$ – the real part of the conductivity dominates, and the conductivity is independent of the wave frequency. This means that the conduction current is in phase with the electric field of the wave. Assuming one conduction electron per atom, a metal such as Fe has an electron–atom collision frequency on the order of 10^{13} s^{-1}. Thus, for microwaves with frequencies $\sim 10^{10}$ s^{-1}, for example, metallic conductivity is essentially real.

In contrast, for frequencies of light from infrared and visible lasers, we can see from equation (3.56) that conductivity is complex and depends strongly on the light wave frequency. The absorption of the electromagnetic wave is governed by the real part of the exponential $\exp(i\mathbf{k}\cdot\mathbf{r})$. The real part of the exponent comes from the imaginary part of k (or, alternatively, n). Thus, if we now substitute the imaginary part of the metallic conductivity given by equation (3.56) into equation (3.49), we can write

$$n^2(\omega, T) = 1 - \frac{\omega_p^2}{\omega^2}\left(1+\frac{\nu_0^2}{\omega^2}\right)^{-1}. \tag{3.57}$$

Here we have assumed electromagnetic wave absorption in a non-magnetic metal, for which $\mu = 1$.

Thus, in computing absorption of laser light in metals, we use equation (3.31) to compute the electron–atom collision frequency ν_0, then use the resulting value of ν_0 in equation (3.57) to compute the index of refraction n, and then finally use the resulting value of n in equation (3.47) to obtain the absorption fraction. We show in Figure 3.4 the absorption fraction computed in this way of 1-μm laser light in Al as a function of temperature.

This prescription is valid, of course, only at very low laser beam intensities, which heat the metal to relatively low temperatures, as shown in Figure 3.4. Once the temperature becomes high enough to ionize the material, bound–free and

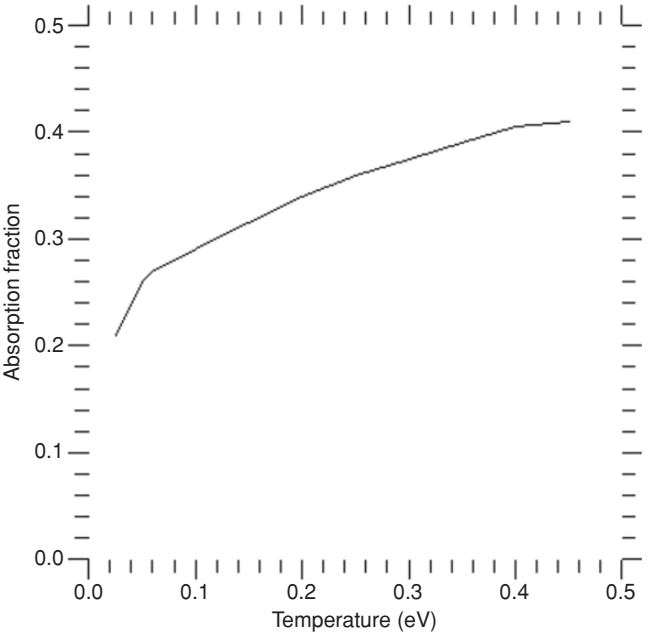

Figure 3.4 Absorption fraction of Al to 1.06-μm laser light as a function of temperature.

free–free absorption mechanisms begin to take over from the bound–bound absorption processes considered here.

Finally, note from equation (3.56) that in classical plasma, where the collision frequency is negligibly small, the conductivity is purely imaginary,

$$\sigma = i\frac{\omega_{pe}^2}{4\pi\omega}. \tag{3.58}$$

This means that the plasma electron current and the electric field are out of phase, so there is no resistive energy loss as there is in a conducting metal. The index of refraction of the collisionless plasma is, from equation (3.57), given by

$$n^2 = 1 - \frac{\omega_{pe}^2}{\omega^2}, \tag{3.59}$$

recovering the relation we presented in Section 3.2.1, equation (3.24), since n^2 is equal to the real part of the dielectric permittivity. We see from equation (3.59) that, for $\omega > \omega_{pe}$, the index of refraction is real and the electromagnetic wave propagates in the plasma. However, for $\omega < \omega_{pe}$, the index of refraction is imaginary and the electromagnetic wave is reflected from the critical density surface, as we discussed in Section 3.2. Note also that for collisionless plasma with a given electron density

and temperature, the conductivity and index of refraction do not depend on the temperature, as they do for a conducting metal, but only on the electron density. In a dynamically evolving plasma being illuminated by a laser beam, however, the electron density changes as the plasma is heated. Thus, in collisionless plasma the position of the absorbing surface changes with time. In a conducting metal being illuminated by very low-intensity laser light, though, the position of the absorption surface remains approximately stationary, but the surface heats up and its absorptivity changes with time.

3.4.3 Absorption in dielectrics and tamped ablation

A dielectric material is a solid composed of atoms that have few or no electrons in the conduction band. These materials are therefore non-conducting.

Let us look back at equation (3.45), the complex wavenumber of an electromagnetic wave propagating in a solid material. For a dielectric, we can assume that the conductivity σ vanishes, so that equation (3.45) becomes

$$k = \sqrt{\mu\epsilon}\frac{\omega}{c}. \tag{3.60}$$

The wavenumber given by equation (3.60) is identical in form to the wavenumber $k = \omega/c$ for an electromagnetic wave traveling in free space (a vacuum). Thus, an electromagnetic wave propagates freely in a dielectric at velocity

$$c' = \frac{c}{\sqrt{\mu\epsilon}}. \tag{3.61}$$

Equation (3.61) is identical to equation (3.20), as it must be, since both are derived directly from Maxwell's equations.

Thus, as long as the laser light has an angular frequency that does not excite any bound–bound transitions, or vibrational or rotational modes of the molecules comprising the neutral material, the dielectric is transparent to the light wave, and has an index of refraction given by

$$n^2 = \mu\epsilon. \tag{3.62}$$

A discussion of refraction and reflection at material surfaces and interfaces is beyond the scope of this book. The interested student can learn much more about refraction and reflection in most texts on optics, like the classic text *Optics* by Max Born and Emil Wolf listed in the Further Reading, and also in the excellent monograph *Radiation Hydrodynamics* by John Castor, also listed in the Further Reading.

As we learned in Chapter 1, most modern lasers have wavelengths in the optical band, wavelengths of 1 μm or less. At these wavelengths, there are many dielectrics

Table 3.1 *Some optically transparent dielectric materials and their optical and thermal properties*

Common name	Chemical symbol	STP density (g cm^{-3})	Thermal conductivity (W m^{-1} K^{-1})	n@λ (μm)	Melt temperature (K)
Acrylic glass	$H_8C_5O_2$	1.182	0.20	1.49@0.61	–
BSO garnet	$Bi_{12}SiO_{20}$	9.194	1.0	2.55@0.63	1163
Barium fluoride	BaF_2	4.83	7.1	1.47@0.59	1627
BK7 glass	SiO_2	2.51	1.11	1.52@0.50	832
Calcium fluoride	CaF_2	3.18	9.71	1.43@0.59	1633
Lexan	$H_{14}C_{16}O_3$	1.196	0.20	1.59@0.55	473
Lithium fluoride	LiF	2.638	11.3	1.39@0.59	1140
Magnesium fluoride	MgF_2	3.176	0.3	1.38@0.59	1528
Sapphire	Al_2O_3	3.98	46	1.77@0.59	2303
Diamond	C	3.51	2200	2.44@0.50	3823
Polyimide	$H_{26}C_{58}N_5O_{11}$	1.43	0.52	1.6@0.66	–

that are completely transparent to the laser light. Optically transparent dielectrics include amorphous materials, such as glass and some polymers, and crystalline materials, such as diamond and sapphire. The common name, chemical formula, STP density, STP thermal conductivity, index of refraction, and melt temperature for several commonly used optically transparent dielectrics are listed in Table 3.1. This table lists only a small fraction of the many optically transparent dielectric materials that are commercially available in a variety of sizes, thicknesses, and crystal orientations, and with a variety of optical and thermal properties. Note that Table 3.1 includes amorphous polymers, such as acrylic glass (also known as PMMA – for poly methyl methacrylate – and also known by its commercial name, Lucite), Lexan (which is the common commercial name for a polycarbonate material), and polyimide; several fluoride crystals; and several gem-stone crystals, such as garnet, sapphire, and diamond. Note also that these materials represent a very wide range of STP thermal conductivities and also melt temperatures. It is meaningless to speak of a melt temperature for an amorphous polymer; we will understand why when we discuss phase transitions in more detail in Chapter 6. The thermal properties of optically transparent dielectrics are important in tamped ablation, which we discuss in more detail below.

There are two circumstances in which a dielectric is not transparent to the laser light. One such circumstance is when the electric field becomes enhanced at some position in the material, like at a metal inclusion or some other impurity in the material, and dielectric breakdown occurs. In dielectric breakdown some free electrons are created at the position of the enhanced field, and then these free

electrons initiate an "avalanche" of collisional ionization that propagates through the dielectric in the direction of the electric field vector, turning the material into plasma along the channel of the ionization wave. The plasma, of course, has very different absorption characteristics to the laser light than does the neutral dielectric.

Natural lightning is triggered by dielectric breakdown of air molecules by the electric field created in a thunderstorm. The storm-produced electric field usually gets enhanced at the tip of some conducting object on the ground, and the ionization wave, or "stepped leader," is then triggered at this point and propagates upward into the cloud. The stepped leader is then followed by an electric current that flows back down and discharges the ionized channel; it is the electric current discharge that we see as the lightning flash. The physics of dielectric breakdown, although a very interesting topic, is also beyond the scope of our discussion here. The interested student is referred to the works listed in the Further Reading.

The other circumstance in which a dielectric is not transparent to laser light is when the photon energy is such that the electromagnetic wave can excite bound–bound electronic transitions in the neutral atoms, or vibrational and rotational modes of the molecules comprising the material. A more detailed discussion of the physics of absorption of laser light via these mechanisms is beyond the scope of this text. We note, however, that very low-intensity far-infrared lasers are used for a variety of material processing applications, including the mitigation of optical glass damage caused by high-intensity laser light in high-power laser systems. In this instance, the glass is transparent to the high-intensity 1- μm or submicron laser light, but absorbs the very-low-intensity infrared (several microns wavelength) laser light, heating it to temperatures close to the glass transition temperature, where the material can then flow and fill in cracks and other damage spots.

Very-low-intensity laser light is also used in a technique of tamped ablation to work-harden metals for a variety of industrial applications and manufacturing processes. In the tamped ablation technique, the ablated plasma produced when the laser beam interacts with the metal is confined, or tamped, by overlaying it with a transparent dielectric. As we learned in Section 3.3, with a 1-μm laser beam one can generate an ~100-kbar pressure pulse in the material with about 10^{11} W cm^{-2} laser beam intensity. This beam intensity can be generated with a few tens of joules from a table-top laser in a spot size of a few millimeters and pulse duration of a few nanoseconds. In contrast, by confining the ablation, it is possible to generate the same 100-kbar pressure pulse with only about 1/100 the unconfined laser intensity, about 10^{9} W cm^{-2}. The lower intensity means that longer pulses and wider spots can be used with the same laser energy. The longer pulse means the pressure pulse can be maintained for a longer time, and can thus penetrate to greater depths in the material. This is of great benefit in materials dynamics studies and in materials

processing applications, like work-hardening of metals, where it is of interest to propagate the pressure pulse over several grain lengths in the material.

In the tamped ablation technique, the material of interest is coated with a thin metallic ablator material, and then, on top of the ablator is placed a thick transparent (to the laser light) dielectric. In some tamped ablation operations, the material, with or without a separate ablator, is placed in a water bath. The water serves in this instance as the transparent dielectric.

As the ablator surface heats up with absorption of the laser light, as discussed in Section 3.4.2, energy thermally conducts back into the dielectric tamper – as well as deeper into the ablator. As the temperature of the dielectric tamper increases, electrons in the valence band below the atom's energy band gap E_g are thermally excited across the band gap into the conduction band, and the conductivity of the dielectric material increases. The conduction band electron density is given by

$$n_e = (\text{constant})\,(kT_e)^{3/2} \exp\left(\frac{E_F - E_g}{kT_e}\right), \tag{3.63}$$

where $E_F < E_g$ is the electron Fermi energy, defined in Section 2.1.3. For covalently bonded dielectrics, like intrinsic semiconductors, $E_F - E_g = -E_g/2$. For most other dielectrics the Fermi energy is not exactly in the middle of the band gap, but assuming that it is turns out to be a reasonably good approximation.

The key fact is that, as the inner edge of the dielectric tamper heats up, the band gap rapidly collapses, the conduction-band electron density increases according to equation (3.63), and the material begins to photo-ionize – that is, the dielectric tamper begins to become opaque to the incident laser light, beginning at the tamper/ablator interface.

The energy of a 1.06-μm photon from a Nd-glass laser is $h\nu = 1.2$ eV, and the ionization potential I of the tamper material, as we will see in Chapter 7, is typically several times larger, in the range 6–15 eV for most atoms and molecules. Thus, a single laser photon cannot ionize the dielectric material; photo-ionization is a multi-photon process. The absorption coefficient for this multi-photon photo-ionization process is given by

$$\kappa\left(\text{cm}^{-1}\right) = 9.14 \times 10^{13} n_0 kT \left(\frac{1.2\text{eV}}{h\nu}\right)^3 \exp\left(\frac{h\nu}{kT}\right)\left[1 - \exp\left(-\frac{h\nu}{kT}\right)\right]^2 \times \exp\left(-\frac{I}{kT}\right), \tag{3.64}$$

where n_0 is the neutral atom density in units of cm^{-3}, and kT is in units of keV. The first exponential term on the right-hand side of equation (3.64) comes from the Planck function, which we derive in Chapter 9; the term in the square brackets

that includes the second exponential accounts for stimulated emission, which we also discuss in Chapter 9; and the third exponential term is from the Saha equation for ionization, which we discuss in more detail in Chapter 7.

Once the material becomes ionized by this multi-photon photo-ionization process, inverse bremsstrahlung absorption and resonance absorption, as discussed in Section 3.2, begin, and soon become the dominant absorption mechanisms of the laser light, just as for high-intensity laser light absorption. Thus, most of the laser energy gets absorbed in the dielectric tamper, near the ablator or sample surface, not in the ablator itself. Indeed, the absorption surface moves outward in time (toward the laser), approximately at the speed of the thermal conduction. Thus, the thermal properties of the dielectric tamper material play a very significant role in the absorption of very-low-intensity laser light in the tamped ablation process. The physics of thermal conduction is discussed in more detail in Chapter 8.

The thermal conduction, as we will see in Chapter 8, depends not only on the temperature of the partially ionized material but also on the electron density. Thus, it is important to account for all processes that change the free electron density in the low-temperature, largely stationary dense plasma, including collisional ionization and three-body recombination. In order to account for these processes, we can solve the following differential equation for the electron density:

$$\frac{dn_e}{dt} = S + \alpha n_e - \beta n_e^2. \tag{3.65}$$

The first term on the right-hand side of equation (3.65) is the free-electron seed rate, the second is the collisional ionization rate, and the third is the three-body recombination rate. In steady-state conditions when there is no external seed, the electron density is given by $n_e = \alpha/\beta$, where the coefficient of the collisional ionization rate, α, can be written

$$\alpha = \frac{(\mathbf{E} \cdot \mathbf{J})\, V}{E_g}. \tag{3.66}$$

Equation (3.66) simply says that the rate at which collisional ionization takes place in a volume V is the inverse of the time required by the electric field to do an amount of work on a free electron, via $\mathbf{E} \cdot \mathbf{J}$ forces, that is equal to the band-gap energy E_g. The three-body recombination rate can be derived from the principle of detailed balance, which we discuss in Chapter 9.

When accounting for all these physical processes we find, as indicated above, that the absorption surface moves outward in the dielectric material approximately linearly with time, and the electron density peaks at the position of this moving absorption surface. In the region between the absorption surface and the surface of the metal ablator or sample, the electron density is depressed, largely as a result of

recombination. The depth into the dielectric material that becomes opaque because of the laser light absorption depends, of course, on the duration of the laser pulse and the thermal properties of the dielectric. Typically, it is only about half a micron per nanosecond of laser pulse duration. Thus, the bulk of the tamper material, both during the laser pulse and after, remains transparent to the laser light. Since the laser energy is deposited not far from the ablator or sample surface, the coupling of stress wave energy into the sample remains relatively efficient throughout the laser illumination. This, of course, is the whole point of tamped ablation.

Finally, it remains for us to determine a relation between laser beam intensity and the resulting pressure. We learned above that the electron density is proportional to the collisional ionization rate, as in equation (3.66). The collisional ionization rate is, in turn, proportional to the electron–neutral collision rate. That collision rate, according to equation (3.51), is proportional to the square-root of temperature. Thus, from relation (3.34), we find

$$P \propto T_e \propto I_L^{1/2}. \tag{3.67}$$

Thus, the pressure created in the dielectric by absorption of the laser light scales as the square-root of the laser intensity. This scaling has been confirmed with detailed simulations, which also show that this scaling holds for laser intensities below about 10^{10} W cm^{-2}, as shown in Figure 3.1. This scaling has also been confirmed by experiment. Note that, unlike for laser intensities greater than 10^{10} W cm^{-2}, there is no dependence of the pressure on the laser wavelength; this is true, of course, only for those laser wavelengths for which the cold dielectric is transparent.

Now that we know how the energy in a laser beam is absorbed in matter, and how this energy gets converted to material pressure, we next turn our attention to how the resulting pressures drive material motions and shock waves. These and related topics are the subject of the next three chapters.

3.5 Example problems and exercises

In doing these problems and exercises, the student can use the thermodynamic and material properties for select materials listed in Appendix III.

Exercise 3.1. Use Maxwell's equations to derive the wave equation for the electric field that is analogous to the wave equation for the magnetic field of equation (3.17).

Exercise 3.2. Use Maxwell's equations to show that, in Gaussian units, the velocity of the electromagnetic wave in a linear, isotropic material with electric permittivity ϵ and magnetic permeability μ is given by equation (3.18).

https://doi.org/10.1017/CBO9781139095150.003 Published online by Cambridge University Press

Exercise 3.3. What is the critical plasma density for 1.06-μm laser light? How does this critical density compare to the solid density of Al? What is the critical density for 10.6-μm laser light? How does this density compare to the solid density of Al? If the coronal plasma in which the laser light is absorbing has an exponential electron density profile with density-gradient scale length $L = n_e/\nabla n_e = 10$ μm, how far from the solid Al surface are the critical density surfaces for the 1.06-μm and 10.6-μm lasers?

Exercise 3.4. How much greater is inverse bremsstrahlung absorption in 0.5-keV plasma than in 1.0-keV plasma?

Exercise 3.5. What is the electron quiver velocity in the electromagnetic field of a laser beam of beam intensity $I_L = 8 \times 10^{15}$ W cm^{-2}? At what electron temperature must hydrogen plasma be for its electrons to have a thermal velocity equal to this quiver velocity?

Exercise 3.6. Replot Figure 3.3 for a laser beam incidence angle of 30° instead of 20°. Does maximum resonance absorption for 30° incidence angle occur at larger or smaller dimensionless density-gradient scale length? By how much?

Exercise 3.7. Derive equation (3.49).

Exercise 3.8. Show that the absorption coefficient for an electromagnetic wave in a metal is basically the reciprocal of the metal's skin depth as given by equation (3.46).

Exercise 3.9. Derive equation (3.57).

Exercise 3.10. The index of refraction of the vacuum (free space) is $n = 1$; for a dielectric it is $n > 1$; for collisionless plasma it is $n < 1$. Whereas a laser beam obliquely entering a dielectric bends toward the normal to the surface, a laser beam obliquely entering collisionless plasma bends away from the normal to the surface. How might we use the refractive properties of plasma to design a "plasma mirror" that will bend the beam back in the direction from whence it came?

Exercise 3.11. In the tamped ablation process, more efficient coupling of the laser beam energy to the sample is obtained when the beam energy deposits in the dielectric tamper closer to the tamper/sample interface. Referring to Table 3.1, which material or materials would make for good tamper material and which would not?

Exercise 3.12. What is the multi-photon photo-ionization absorption coefficient for very-low-intensity 1.06-μm laser light in BK7 glass at 1-eV temperature?

Exercise 3.13. Since pressure achieved in the tamped ablation process is a weak function of laser intensity – that is, $P \propto I_L^{1/2}$ – pressures are limited by the intensity threshold for dielectric breakdown of the tamper material. Thus, purity of the material is very important. Artificially grown optical crystals typically have a higher breakdown threshold than natural gem stones or glass. If it is possible to achieve 100-kbar pressure in CaF_2 with 4×10^{10} W cm^{-2} laser light, what is the maximum pressure we can achieve in a different optically transparent dielectric that has a dielectric breakdown threshold of 10^{10} W cm^{-2} and 4×10^9 W cm^{-2}?

https://doi.org/10.1017/CBO9781139095150.003 Published online by Cambridge University Press